Autonomous Actuation of Flapping Wing Robots Inspired by Asynchronous Insect Muscle

James Lynch[1], Jeff Gau[2], Simon Sponberg[2], and Nick Gravish[1]

***Abstract*— In most instances, flapping wing robots have emulated the "synchronous" actuation of insects in which the wingbeat timing is generated from a time-dependent, rhythmic signal. An understudied area in flapping wing robotics is that of "asynchronous" actuation in which the wingbeat is self-excited through state-dependent feedback. The internal dynamics of asynchronous insect flight muscle enable high-frequency, adaptive wingbeats with minimal direct neural control. In this paper, we investigate how the delayed stretch-activation (dSA) response of asynchronous insect flight muscle can be transformed into a feedback control law for flapping wing robots that results in stable limit cycle wingbeats. We first demonstrate in theory and simulation the mechanism by which asynchronous wingbeats self-excite. Then, we implement the feedback law on a dynamically-scaled robophysical model as well as on an insect-scale robotic flapping wing. Experiments on the large- and small-scale robots demonstrate good agreement with the theory results and highlight how dSA parameters govern wingbeat amplitude and frequency. Lastly, we demonstrate that asynchronous actuation has several advantages over synchronous actuation schemes, including the ability to rapidly adapt or halt wingbeats in response to external loads or collisions through low-level feedback control.**

I. INTRODUCTION

The field of bioinspired flapping-wing micro-air vehicles (FWMAVs) has seen major advancements in the last decade. Researchers have achieved controlled flight on tethered [1], [2] and untethered [3]–[6] FWMAVs at the centimeter scale. They have integrated sensors [7]–[10] and implemented robots with a wide range of actuators including piezo bending actuators, mini DC motors [11]–[13], soft DEA actuators [14], and electromagnetic coils [15]. Others have developed autonomous control algorithms that (given sufficient knowledge of the state of the robot) can achieve not just stable hovering, but also impressive feats of agility [16]. The design, fabrication, and control tools now exist to design novel FWMAVs capable of flight.

However, the performance of such robots still lags behind that of their insect muses. The agility and versatility of insects like flies, bees, and dragonflies is unmatched by any FWMAV at similar scales. Untethered FWMAVs at the centimeter scale must be supplied with extremely high-power energy sources—lasers [17] or high-wattage light sources [3]—while insects are efficient enough to sustain flight over long distances during foraging and migration [18], [19]. Additionally, FWMAVs are often much more delicate than insects, constructed of 100-micron-thick carbon fiber, thin polymer sheets, and brittle piezoelectric materials. The dynamics of flight are sensitive to changes in mechanical properties (wing geometry, inertia, etc.), and yet insects are able to continue to fly despite damage caused by the environment or other animals [20], [21]. There is still much for us to learn about how insects achieve their impressive flight performance and translate these into advances in robotics.

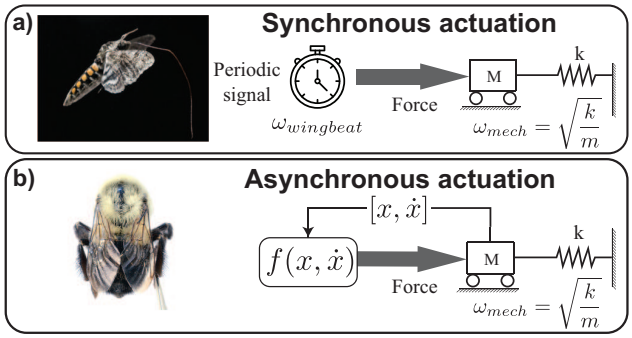

Fig. 1. a) Insects such as moths use synchronous actuation. This is characterized by a periodic signal from an internal source with rate $\omega_{wingbeat}$. b) Bumblebees are an example of an insect using asynchronous actuation. This is characterized by feedback, where the rate of the mechanical system ω_{mech} interacts with the rate of the feedback $\omega_{feedback}$ to produce the wingbeat.

Flapping wing insects can be classified into one of two actuation strategies: synchronous and asynchronous (Fig. 1). Insects such as moths generate wingbeats through a periodic signal generated by the nervous system that is "synchronous" with the wingbeat, while insects such as bees rely on a strain-dependent response of the muscle to generate self-excited wingbeats whose frequency is higher than signals from the nervous system and therefore "asynchronous" from the neural signals. Asynchronous muscle actuation is thought to provide several distinct advantages to flying insects including: high wingbeat frequency (wbf), adaptive behavior after wing damage [22], and separation of power and control. [23]–[25]. To the authors knowledge, all previous actuation of flapping wing robots have relied on synchronous actuation strategies. We hypothesize that asynchronous actuation methods provide adaptive behaviors that could be beneficial for flapping wing robots.

A key specialization in asynchronous muscle is a phenomenon called *delayed stretch activation* (dSA), wherein, after the muscle is stretched, its force will continue to increase, reaching a peak that is delayed in time w.r.t. the stretch. (Fig 2a). Due the time delay in stretch-activated

*This work was supported by the National Science Foundation under Grant No. 2100858.

James Lynch and Nick Gravish are with the [1]Department of Mechanical and Aerospace Engineering, University of California, San Diego. Email {jelynch, ngravish}@eng.ucsd.edu. Jeff Gau and Simon Sponberg are with the [2]School of Physics, Georgia Institute of Technology, Atlanta, GA. Email {jeff.gau, sponberg}@gatech.edu

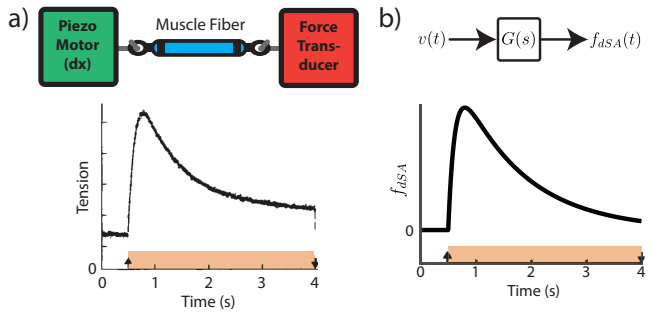

Fig. 2. a) The force activation response of the muscle of a giant water bug to a step strain. Data adapted from [25] and muscle diagram adapted from [33]. b) The response of the dSA transfer function to a strain-rate impulse is qualitatively similar given the right choices of μ, r_3, and κ.

peak force, two such muscles arranged antagonistically in the insect thorax tend to naturally oscillate, flapping the wings with *no direct input* from the nervous system. Biologists have studied asynchronous muscle in isolation by carefully removing the muscles from the insect thorax and applying techniques adapted from materials science such as measuring cyclic force-displacement, and force response to position step inputs [26]–[28]. Their results have been used to characterize asynchronous muscle as an active material and compare muscle behavior across species [25] and between lines of transgenic flies [29]. However, biologists have been typically interested in the elusive bio-molecular dynamics from which the dSA phenomenon arises. To enable asynchronous actuation in FWMAVs, it is necessary to characterize the system level behavior of asynchronous flight: the dynamical interactions between asynchronous muscle, the elastic thorax [30] and the complex aerodynamic forces on the wing [31].

In this manuscript we seek to establish principles of asynchronous actuation for flapping wing robots and to demonstrate some unique properties of dSA actuation for adaptive and resilient flapping wing dynamics. We begin by deriving the dynamical equations for dSA and show that it is dynamically similar to a second-order low-pass filter on the strain rate of the muscle. We then integrate the dSA feedback law with the nonlinear equations of motion of a "spring-wing" system with aerodynamic drag and elastic energy storage [32]. Using the equations of motion, we derive conditions for the existence of stable limit cycles and use a combination of simulation and robophysical model experiments as validation. We present experiments in the robophysical model that show that an asynchronously-actuated robot has a compelling ability to rapidly adapt wingbeat properties and respond to collisions with no direct control. Lastly, we implement dSA feedback in an insect-scale flapping wing as a proof of concept towards creating a full asynchronous FWMAV.

II. The Dynamics of DSA

The first step towards integrating dSA into a robotic flapping system is to express the observed behavior of asynchrononus muscle as a function of the state of the system. The time-dependent force response (f_{step}) of the muscle to a step change in its length (see Fig. 2a) has been parameterized as the sum of three exponents [33]:

$$f_{step}(t) = K_2 e^{-r_2 t} + K_3(1 - e^{-r_3 t}) + K_4 e^{-r_4 t} + c \quad (1)$$

Each term corresponds to a phase of the response: An extremely fast decay ($r_2 >>$ wbf), a slower rise ($r_3 \approx$ wbf), and a very slow decay ($r_4 <<$ wbf). The constant c represents the passive stiffness of the muscle. This 7-term model is fitted to stretch-and-hold data collected from insect muscle fibers and used to evaluate the behavior of the muscle.

To ease the complexity of analyzing the behavior of a system with dSA forcing, we focus on the Phase 3 and 4 dynamics, which are of the same order as the wbf [25]. We choose to focus on the r_3 term in particular because it has been shown to vary linearly with wbf across a range of insects [25]. The very fast dSA dynamics (Phase 2) are effectively damped out by the spring-mass-damper dynamics of an elastic flapping wing. Setting $K_3 = K_4 = 1$, $c = 1$, and defining the ratio of the slower rates, $\kappa = r_4/r_3$, we can write:

$$f_{step}(t) = -e^{-r_3 t} + e^{-\kappa r_3 t} \quad (2)$$

Since $r_4 > r_3$, $\kappa < 1$, and typically is in the range of $0.01 - 0.3$ in insects [25]. By tuning r_3 and κ and adjusting the peak amplitude via a muscle "strength" term, μ, we can match the shape of the asynchronous muscle response (Fig. 2b).

A. A Linear Systems Model of the dSA phenomenon

The expression in Eq. 2 is the response of the system to a step in the muscle strain, which is equivalent to an impulse in the strain rate. This implies that Eq. 2 is the *impulse response of the muscle given strain rate as the input*. We can express the forcing function as a convolution of the impulse response with the strain rate,

$$f_{dSA}(t) = g(t) * v(t) \triangleq \int_0^\infty g(\tau) v(t - \tau) d\tau \quad (3)$$

where $g(t) = -e^{-r_3 t} + e^{-\kappa r_3 t}$.

In the Laplace domain, convolution is a straightforward multiplication rather than an integration, i.e. $F_{dSA}(s) = G(s)V(s)$. Taking the Laplace transform of the response function $g(t)$ as defined in Eq. 2, we get the transfer function $G(s)$ which transforms the velocity feedback input to the dSA forcing output:

$$\begin{aligned} \mathcal{L}(g(t)) = G(s) &= \frac{r_3(1-\kappa)}{s^2 + r_3(1+\kappa)s + \kappa r_3^2} \\ &= \frac{\alpha_1}{s^2 + \alpha_2 s + \alpha_3} \end{aligned} \quad (4)$$

where we've defined 3 parameters, α_1, α_2, and α_3 for convenience. The dSA phenomenon, therefore, is qualitatively similar to a second-order low-pass filter on the velocity, fed back to the muscle as a force command.

B. The asynchronous spring-wing system equations

The Laplace representation of dSA is useful in that it allows us to express the dynamics of asynchronous actuation

as an ODE. In the Laplace domain, the force output is the product of the transfer function and the velocity input:

$$F_{dSA}(s) = \left[\frac{\alpha_1}{s^2 + \alpha_2 s + \alpha_3}\right] V(s) = G_{dSA}(s)V(s) \quad (5)$$

We can distribute the denominator of $G(s)$ and take the inverse Laplace transform:

$$s^2 F_{dSA}(s) + \alpha_2 s F_{dSA}(s) + \alpha_3 F_{dSA}(s) = \alpha_1 V(s) \quad (6)$$

$$\mathcal{L}^{-1} \Rightarrow \ddot{f}_{dSA} + \alpha_2 \dot{f}_{dSA} + \alpha_3 f_{dSA} = \alpha_1 v \quad (7)$$

To connect the dSA actuation dynamics to the inertial, elastic, and aerodynamic elements of the flight system, we use the nonlinear "spring-wing" equation that is commonly used [32], [34], [35] to describe flapping systems with internal elasticity. The equations of motion in terms of inertia I, stiffness k, drag torque term Γ, and the applied torque $\tau_{applied}$:

$$I\ddot{\theta} + k\theta + \Gamma|\dot{\theta}|\dot{\theta} = \tau_{applied} \quad (8)$$

The asynchronous muscle dynamics dictate the torque applied to the system and are scaled by a gain coefficient, μ (units: Nm rad^{-1}), so we may write the combined equations of motion:

$$\begin{aligned} m\ddot{\theta} + k\theta + \Gamma|\dot{\theta}|\dot{\theta} - \mu f_{dSA} &= 0 \\ \ddot{f}_{dSA} + \alpha_2 \dot{f}_{dSA} + \alpha_3 f_{dSA} - \alpha_1 \dot{\theta} &= 0 \end{aligned} \quad (9)$$

Solving these equations simultaneously gives the trajectory of the flapping wing, $\theta(t)$. The prevalence of asynchronous insects that employ dSA actuation suggests that this system can produce stable limit cycle oscillations from the balance between quadratic aerodynamic damping and strain-rate dependent muscle actuation. However, this is not guaranteed. To evaluate whether dSA is suitable for actuating a robot we must study the dynamical behaviors of this system. For example, there may exist combinations of feedback and mechanical parameters that *do not* result in oscillations, or other regimes in which more exotic dynamical behaviors appear (exponential growth, chaos, etc.) that should be avoided in a robot implementation. It is necessary to identify the conditions under which a stable limit cycle can be expected to form.

C. Asynchronous wingbeats result from a linear instability

The stationary state, $[\theta, \dot{\theta}, f_{dSA}, \dot{f}_{dSA}] = 0$, is a fixed point of the asynchronous dynamical system (Eq. 9). We now seek to understand if this fixed point is stable or unstable. We ask the following question: if there is a small perturbation to the closed-loop system with dSA feedback, will oscillations tend to decay back to the origin or will they grow?

The system described in Eqs. 9 is nonlinear and so we can define a new state vector $\boldsymbol{\sigma} = [\theta, \dot{\theta}, f_{dSA}, \dot{f}_{dSA}]$

$$\begin{aligned} \dot{\sigma}_1 &= \sigma_2 \\ \dot{\sigma}_2 &= -\tfrac{k}{m}\sigma_1 - \Gamma|\sigma_2|\sigma_2 + \tfrac{\mu}{m}\sigma_3 \\ \dot{\sigma}_3 &= \sigma_4 \\ \dot{\sigma}_4 &= \alpha_1\sigma_2 - \alpha_3\sigma_3 - \alpha_2\sigma_4 \end{aligned} \quad (10)$$

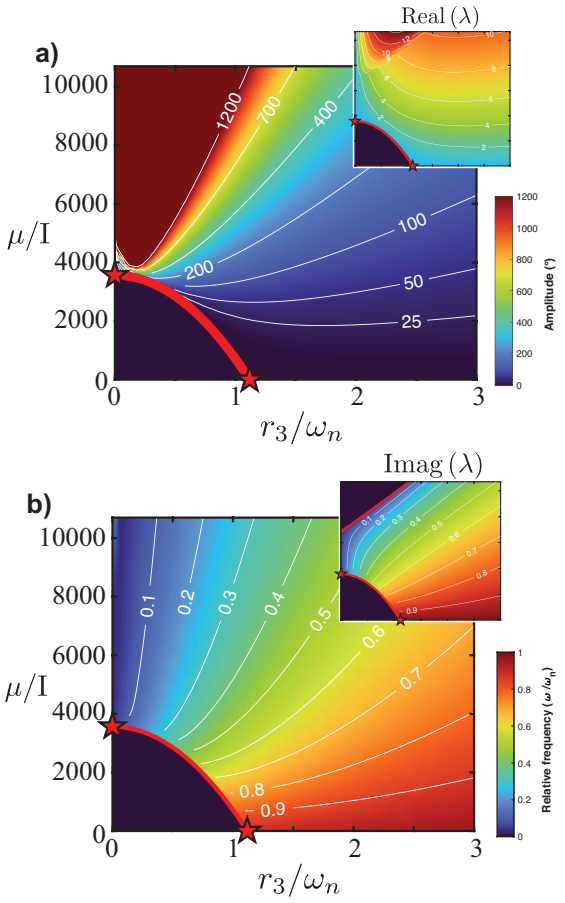

Fig. 3. Plots of amplitude and frequency of dSA limit-cycle oscillations as a function of r_3/ω_n and μ/I. Red lines indicate calculated stability boundaries separating stable limit-cycle oscillations (large μ, r_3) from stationary behavior (small μ, r_3) from equation 14. Stars indicate the x- and y-intercepts of the stability curve, (Eq.16). a) Amplitude of oscillation grows with increasing μ and non-monotonically varies with r_3. Inset shows the real component of the eigenvalue of the linearized system which shows qualitative agreement with the non-linear system. b) Frequency decreases with increasing both μ and r_3.

We next linearize about the point $\boldsymbol{\sigma} = 0$, constructing the Jacobian and the linear dynamics about the stationary state:

$$\dot{\boldsymbol{\sigma}} = \begin{bmatrix} 0 & 1 & 0 & 0 \\ -\frac{k}{m} & 0 & \frac{\mu}{m} & 0 \\ 0 & 0 & 0 & 1 \\ 0 & \alpha_1 & -\alpha_3 & -\alpha_2 \end{bmatrix} \boldsymbol{\sigma} \quad (11)$$

The growth or decay of perturbations from the stationary state are determined by the eigenvalues of the Jacobian. The characteristic equation for the linear system is

$$\lambda^4 + \alpha_2\lambda^3 + (\frac{k}{m} + \alpha_3)\lambda^2 + (\frac{k}{m}\alpha_2 - \frac{\mu}{m}\alpha_1)\lambda + \frac{k}{m}\alpha_3 = 0 \quad (12)$$

with eigenvalues $\lambda_j = a_j + i\omega_j$.

The sign of the real part of the largest eigenvalue dictates whether a perturbation away from the stationary point will tend to decay (stable) or grow (unstable). Understanding the conditions on the stability boundary will enable us to choose relevant feedback parameters to induce oscillations.

We can determine the boundary between decaying and growing solutions by setting the real part of the eigenvalue

to zero, e.g. $\lambda = i\omega$, where ω is the frequency of oscillation. Plugging in for λ and separating the real and imaginary parts, we get two equations:

$$\begin{aligned} \textbf{Real :} \quad & \omega^4 - (\tfrac{k}{I} + \alpha_3)\omega^2 + \tfrac{k}{I}\alpha_3 \quad = 0 \\ \textbf{Imag :} \quad & \tfrac{k}{I}\alpha_2 - \tfrac{\mu}{I}\alpha_1 - \alpha_2\omega^2 \quad = 0 \end{aligned} \tag{13}$$

We are specifically interested in how the parameters, μ and r_3, influence the onset of asynchronous oscillations due to the instability of the stationary point. Recall the definitions of the coefficients, $\alpha_1 = r_3(1-\kappa)$, $\alpha_2 = r_3(1+\kappa)$, $\alpha_3 = \kappa r_3^2$. We also define $\omega_n^2 = k/I$ as the natural frequency of the system and $\hat{\mu} = \mu/I$.

The first equation is quadratic in ω^2. Solving, we get two solutions: $\omega^2 = \kappa r_3^2$ and $\omega^2 = \omega_n^2$. Plugging each into the second equation, we get a pair of equations:

$$\oplus \rightarrow \hat{\mu} = \frac{1+\kappa}{1-\kappa}(\omega_n^2 - \kappa r_3^2) \tag{14}$$

$$\ominus \rightarrow \hat{\mu} = 0 \tag{15}$$

Eq. 15 gives the trivial conditions (zero feedback gain = no oscillations), but Eq. 14 defines a relationship between the strength of the dSA feedback and its rate parameter, plotted in Fig. 3 (red line). The two equations define 4 quadrants in the $r_3 - \mu$ plane where perturbations tend to either grow or decay. In the current work, we'll focus just on the two regions that exist for $\mu > 0$.

D. Emergence and properties of dSA limit cycles

In the previous section we demonstrated that for certain dSA parameters the stationary state is unstable and oscillations will grow. In a system with quadratic damping, a stable limit cycle may form where the system oscillates such that the energy input from the muscle over one period exactly balances the energy dissipated by the environment. In order to control flapping oscillations, we need to understand how the amplitude and frequency of oscillations vary with the system parameters. The nonlinear aerodynamic damping presents challenges to deriving analytical solutions of the system. However, we can study the behavior of the system via numerical simulation.

We simulated the nonlinear equations of motion from Eq. 10 in Matlab (R2021a, Mathworks) using the ode45 solver. We chose mechanical parameters (k, I, Γ) that matched those of a robophysical experimental system that we will use section III. We selected 0.8 as an arbitrary value for κ and the results are independent of this choice. We computed intercepts of Eq. 14,

$$r_3^* = \frac{\omega_n}{\sqrt{\kappa}}, \qquad \hat{\mu}^* = \frac{1+\kappa}{1-\kappa}\omega_n^2 \tag{16}$$

and defined ranges of $\hat{\mu}$ and r_3 from 0 to 3 times the intercept value. We ran simulations at each configuration and computed the amplitude and frequency of oscillations, which were typically sinusoidal. The results are shown in Fig. 3.

Our simulations confirm that the stability boundary in Eq. 14 does divide the plane into oscillatory and non-oscillatory regions. Additionally, there is a clear trend that shows that increasing $\hat{\mu}$ leads to an increase in flapping amplitude and a decrease in flapping frequency. The change in frequency is predicted by linear eigenvalue analysis (Fig. 3b, inset). However, when amplitudes get very high (high $\hat{\mu}$), nonlinear drag effects become more significant, causing the lines of constant frequency to deviate from the linear predictions. This discrepancy underlines the importance of considering the inherent nonlinearity of the system.

It is important to note that many of the solutions shown in Fig. 3 are simply impractical. At high-$\hat{\mu}$, low r_3, we see oscillation amplitudes well above 360 degrees, whereas a hinge on a flapping robot would be expected to have a maximum angle of only ~90 degrees. This limitation, in addition to limits on the torque and max displacement of a potential actuator, means that in practice, dSA feedback will need to have a relatively small $\hat{\mu}$.

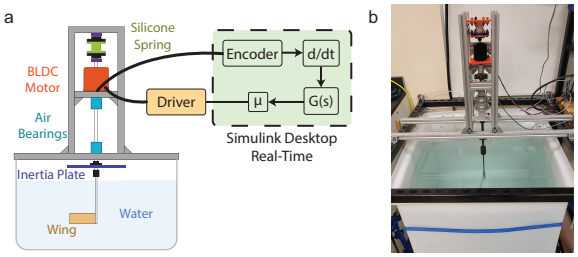

Fig. 4. a) Diagram of the dynamically-scaled robotic model and control scheme. b) A photo of the system

III. Implementation in a Scaled Robotic Model

In this section we describe experiments on a dynamically-scaled robotic flapping wing, which we call a robophysical system since it employs robotics and feedback coupled to physical and environmental forces. The robophysical system has well characterized mechanical parameters and is easily modified thanks to its modular design, enabling a range of tests that would be more difficult at a smaller scale.

A. Design of an asynchronous robotic spring-wing

The robophysical system we use in this study (Fig. 4) was adapted from a similar system described in [32]. It consists of an elastic element (a molded silicone torsion spring), a main shaft supported by a thrust bearing and radial air bearings, an optical rotary encoder (4096 CPR, US Digital), and a rigid, fixed-pitch acrylic wing in water. The inertia can be changed by fixing one of a set of inertia plates to the main shaft. Data collection and control of the system is done via a DAQ (PCIe 6323, NI) and Simulink Desktop Real-Time (SLDRT) (Mathworks), which enables hardware-in-the-loop control at a rate of 1000 samples/s.

The key feature of the asynchronous robotic model is the method of driving the system. We use a brushless DC motor (D6374 150KV, ODrive Robotics) and a motor driver to capable of closed-loop torque control at 10 kHz. The angular position of the wing is used as the input to a SLDRT model that implements the dSA transfer function (Eq. 4), multiplies

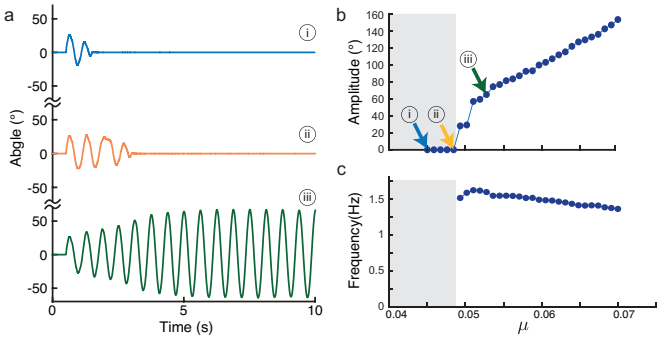

Fig. 5. Results of increasing μ while keeping the mechanical parameters and r_3 constant ($k = 416$Nm rad^{-1}, $I = 1.96 \times 10^{-3}$kg m^2, $r_3 = 35$s^{-1}, and $\kappa = 0.5$). a) Three representative plots in the time domain: no oscillation (μ too low), a borderline case, and stable oscillations (μ large enough). b) The amplitude of oscillation increases as μ increases, and the frequency decreases slightly.

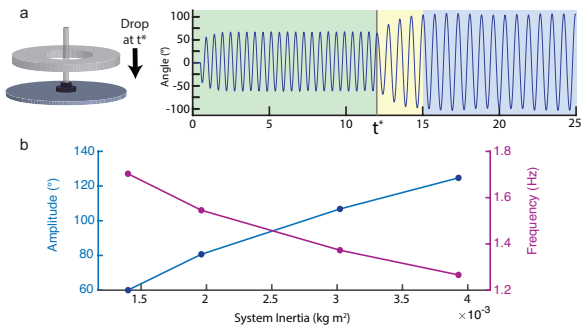

Fig. 6. The asynchronous spring-wing adapts to changes in its mechanical system properties. a) When extra mass is added to the inertia plate on the large-scale robot model, the system transitions to a new amplitude and frequency. b) When we varied the inertia over a large range, we saw that increasing inertia decreases the frequency and increases the amplitude of the wingbeat

the output by the strength, μ, and sends a torque command to the motor via USB, as shown in Fig. 4a. The direct torque control method eliminates the need to explicitly integrate the motor dynamics into the asynchronous ODE.

B. Controlling amplitude and frequency in a real system

We tested the effect of changing the value of μ in the robotic model while holding r_3 constant. The system parameters are as follows: Stiffness $k = 0.416$ Nm rad^{-1}, Inertia $I = 1.96 \times 10^{-3}$ kg m^2, $r_3 = 35s^{-1} = 2.4\omega_n$, and $\kappa = 0.5$. The value of r_3 places this configuration on the side of the stability boundary that should mean that it oscillates as long as $\mu > 0$. However, when we choose a small value for μ, we find that an initial perturbation actually tends to decay back to zero (Fig. 5a-i). In this case, the dSA feedback is not strong enough to overcome the effects of friction in the bearings. We don't model friction in our simulations, but we can see that as $\hat{\mu} \to 0$ in Fig. 3a, the oscillation amplitude approaches zero. When friction is present in the system, arbitrarily small amplitudes are not possible, so the oscillation decays. Increasing μ leads to a "borderline" case where the system oscillates for a few periods before decaying again (Fig. 5a-ii). When μ finally crosses the threshold, stable oscillations result from an initial perturbation. We observe a roughly linear relationship between μ and amplitude, as well as a subtle decrease in oscillation frequency with increasing μ (Fig. 5, b and c)

C. Exemplary behaviors of dSA flapping wing systems

Beyond the control of flapping amplitude and frequency, we are able to examine novel behaviors of dSA flapping wing systems via the robophysical model. We observed that the asynchronous system was able to naturally adapt to changes in its mechanical properties. Additionally, the system features an extremely fast response to collisions with environmental obstacles, reducing the potential for serious damage to the wings or wing transmission.

1) Adaptation to changing mechanical parameters: Figure 6a shows the results of an experiment where additional mass is added to an inertia plate during an experiment. One might expect that the addition of extra inertia would cause the amplitude to decrease, as the motor now needs to move more mass. However, we see that as soon as the inertia of the system changes at $t = t^*$, the asynchronous flapper adjusts to the new loads on the system, actually increasing in amplitude and decreasing frequency. It *adapts* to the new system properties. Keeping the same values of r_3 and μ, we measured amplitude and frequency of oscillation for 4 different inertias. Figure 6b shows that this trend continues for higher inertias, suggesting that the product of amplitude and frequency remains roughly constant.

A robot with an adaptive control scheme like this is able to respond to changes to its mechanical properties automatically. This qualitatively has similarity to the adaptive oscillators explored for legged-locomotion, in which robots adjust gait and frequency when loads are added [36]. Damage to a wing or accumulation of debris may cause changes in wing inertia that would seriously impact the performance of a synchronously driven robot whose frequency is dictated by the resonance curve of the robot [37]. An asynchronously-driven robot, on the other hand, would simply adapt to a new frequency and amplitude that would still enable it to fly. As FWMAVs move from safe laboratory conditions to the more unpredictable world-at-large, adaptation to new situations will be ever more critical.

2) Fast response to collisions with the environment: Another inevitable consequence of operating in unstructured environments is collisions. The brittle actuator materials and delicate microstructures that make up typical FWMAVs make it all the more important to avoid or mediate damage from collisions. We wanted to investigate the response of the asynchronous system to a collision with a rigid object in the environment.

We fixed an inertia plate to the robotic model that included vertical posts and set the system to oscillate. At $t = t^*$, we interrupted the motion of the system by causing a post to collide with an obstacle. We observed that the system stopped almost immediately, well within a single period (Fig.

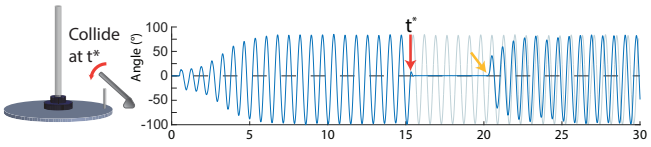

Fig. 7. When the system collides with an obstacle at $t = t^*$, it naturally stops thanks to the dSA feedback law. It easily starts up again later as any small perturbation grows back to the original limit cycle

7). Very shortly after the angular velocity is reduced to zero, the dSA feedback also goes to zero, causing the actuator to stop driving the wing.

In the synchronous forcing case, represented by the light-colored trace in Fig. 7, the actuator is oblivious to the collision and continues to apply torque to the wing after it has already stopped, potentially causing damage to the wing structure. The low-level feedback inherent to asynchronous actuation enables the system to respond immediately, reducing the potential for damage. In addition, as soon as the system is perturbed again, after it is clear of the obstacle, it resumes flapping at the same amplitude and frequency. The asynchronous system naturally avoids damage and does it within a single oscillation period with no need for an explicit command to stop actuation. It may serve as a sort of distributed control, offloading some need for the flight controller to respond to environmental disturbances.

IV. Insect-scale asynchronous flapping wing

As a proof-of-concept demonstration, we implemented dSA feedback on an insect-scale robotic wing. The wing apparatus, consisting of a thin polymer wing (15mm x 5mm x 0.1mm) supported by a carbon fiber frame, a PZT bimorph bending actuator, and a transmission, is based on the design from [1] (see Fig. 8a). Here, we used just a single wing, supported by acrylic brackets instead of a carbon fiber airframe. We aligned a fiber optic displacement sensor (D21, Philtec) with the tip of the actuator to track the actuator displacement. Oscillations were induced by an aerodynamic perturbation provided by a toy vortex ring gun (Zero Blaster, zerotoys.com). We recorded high speed video of the system from the top down as the vortex crossed the wing. Frames from the video can be seen in Fig. 8b.

The output from the displacement sensor was fed into an NI DAQ (PCIe 6343) and used as input the same SLDRT model that implemented the dSA feedback law described in previous Section III. Typically, PZT bimorph actuators are driven by providing 3 voltage signals: a high-voltage bias (250V) on one side of the bimorph, a control signal (0V-250V) in the middle, and ground on the other side. Bending in the actuator is driven by the electrical potential between the signal and the two sides of the bimorph. To close the loop via dSA feedback, we took the derivative of the displacement to get velocity and fed the velocity into the dSA transfer function 4 with $r_3 = 225$ Hz ($\sim 3\omega_n$). The output was converted to voltage and fed through an amplifier to the PZT control signal. As with the large-scale robotic model, we slowly increased μ until stable oscillations were observed. Fig. 8 shows the result of two tests: one with μ too small to

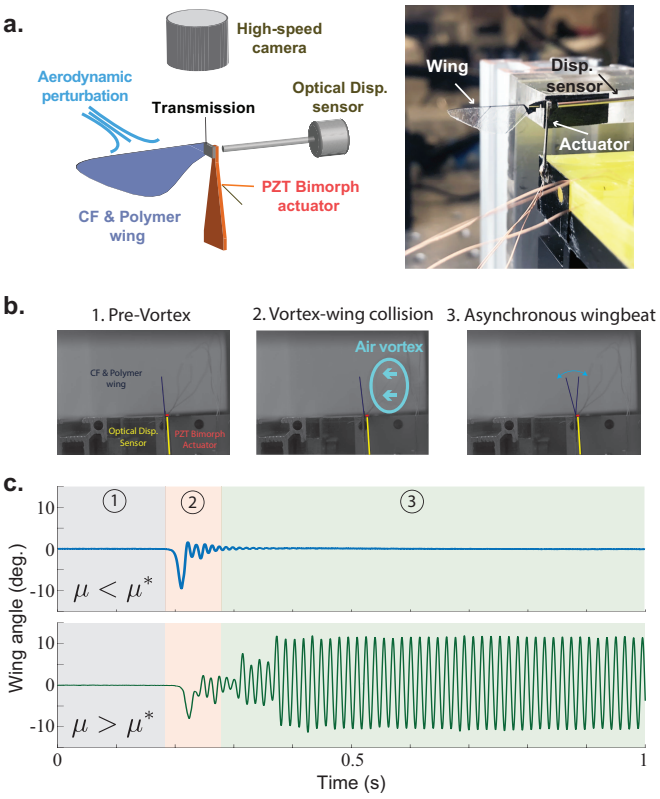

Fig. 8. a) Robobee wing experiment diagram, side and top views and photo of the setup. b) High-speed video stills before, during, and after vortex perturbation. c) Wingbeat dynamics when μ value is too low (top) and when μ is increased above the oscillation threshold (bottom). Numbered regions correspond to the images in b.

overcome friction, and one with a large enough μ to induce oscillations. Larger values of μ may have provided larger amplitudes, but we used this minimum μ value in our testing to avoid overloading the actuator and the robot.

V. Conclusion & Future Work

In this paper we derive and study the first dynamical system representation of asynchronous wingbeat actuation in flapping wing robots and insects. The dSA feedback control law that we have described here is a novel method of achieving flapping in robots. Asynchronous actuation in current FWMAVs is simple to implement and requires only 1) a state estimate via strain gauge, encoder, gyroscope, or other sensor and 2) knowledge of the internal dynamics of the actuator. The method can be applied to a wide range of actuators using relatively simple analog hardware or simple digital logic. The resulting system naturally oscillates powered and can be controlled by adjusting the feedback parameters OR by changing the mechanical properties (e.g. wing inertia) of the robot.

While our implementation of asynchronous actuation relied on actuators, sensors, and a feedback loop, the dSA response of insect flight muscle is “material” property of the muscle. Thus asynchronous wingbeats emerge from the lowest level of mechanical feedback within asynchronous insects. Future work to engineer such low-level feedback properties into active materials and circuits will be of great interest for future FWMAVs.

REFERENCES

[1] Kevin Y. Ma, Pakpong Chirarattananon, Sawyer B. Fuller, and Robert J. Wood. Controlled Flight of a Biologically Inspired, Insect-Scale Robot. *Science*, May 2013. Publisher: American Association for the Advancement of Science.

[2] Zhan Tu, Fan Fei, Jian Zhang, and Xinyan Deng. Acting Is Seeing: Navigating Tight Space Using Flapping Wings. In *2019 International Conference on Robotics and Automation (ICRA)*, pages 95–101, May 2019. ISSN: 2577-087X.

[3] Noah T. Jafferis, E. Farrell Helbling, Michael Karpelson, and Robert J. Wood. Untethered flight of an insect-sized flapping-wing microscale aerial vehicle. *Nature*, 570(7762):491–495, June 2019.

[4] G.C.H.E. de Croon, K.M.E. de Clercq, R. Ruijsink, B. Remes, and C. de Wagter. Design, Aerodynamics, and Vision-Based Control of the DelFly. *International Journal of Micro Air Vehicles*, 1(2):71–97, June 2009.

[5] Matthew Keennon, Karl Klingebiel, and Henry Won. Development of the Nano Hummingbird: A Tailless Flapping Wing Micro Air Vehicle. Nashville, Tennessee, 2012. AIAA.

[6] Zhan Tu, Fan Fei, and Xinyan Deng. Untethered Flight of an At-Scale Dual-Motor Hummingbird Robot With Bio-Inspired Decoupled Wings. *IEEE Robotics and Automation Letters*, 5(3):4194–4201, July 2020. Conference Name: IEEE Robotics and Automation Letters.

[7] Sawyer B. Fuller, Michael Karpelson, Andrea Censi, Kevin Y. Ma, and Robert J. Wood. Controlling free flight of a robotic fly using an onboard vision sensor inspired by insect ocelli. *Journal of The Royal Society Interface*, 11(97):20140281, August 2014. Publisher: Royal Society.

[8] Kaushik Jayaram, Noah T. Jafferis, Neel Doshi, Ben Goldberg, and Robert J. Wood. Concomitant sensing and actuation for piezoelectric microrobots. *Smart Materials and Structures*, 27(6):065028, May 2018. Publisher: IOP Publishing.

[9] C. De Wagter, S. Tijmons, B. D. W. Remes, and G. C. H. E. de Croon. Autonomous flight of a 20-gram Flapping Wing MAV with a 4-gram onboard stereo vision system. In *2014 IEEE International Conference on Robotics and Automation (ICRA)*, pages 4982–4987, Hong Kong, China, May 2014. IEEE.

[10] Kevin Y. Ma, Pakpong Chirarattananon, and Robert J. Wood. Design and fabrication of an insect-scale flying robot for control autonomy. In *2015 IEEE/RSJ International Conference on Intelligent Robots and Systems (IROS)*, pages 1558–1564, September 2015.

[11] Domenico Campolo, Muhammad Azhar, Gih-Keong Lau, and Metin Sitti. Can DC Motors Directly Drive Flapping Wings at High Frequency and Large Wing Strokes? *IEEE/ASME Transactions on Mechatronics*, 19(1):109–120, February 2014.

[12] Muhammad Azhar, Domenico Campolo, Gih-Keong Lau, and Metin Sitti. Flapping Wings with DC-Motors via Direct, Elastic Transmissions. *Proceedings of International Conference on Intelligent Unmanned Systems*, 8(0), 2012. Number: 0.

[13] Muhammad Azhar, Domenico Campolo, Gih-Keong Lau, Lindsey Hines, and Metin Sitti. Flapping wings via direct-driving by DC motors. In *2013 IEEE International Conference on Robotics and Automation*, pages 1397–1402, May 2013. ISSN: 1050-4729.

[14] Yufeng Chen, Huichan Zhao, Jie Mao, Pakpong Chirarattananon, E. Farrell Helbling, Nak-seung Patrick Hyun, David R. Clarke, and Robert J. Wood. Controlled flight of a microrobot powered by soft artificial muscles. *Nature*, 575(7782):324–329, November 2019. Number: 7782 Publisher: Nature Publishing Group.

[15] Jesse A. Roll, Bo Cheng, and Xinyan Deng. An Electromagnetic Actuator for High-Frequency Flapping-Wing Microair Vehicles. *IEEE Transactions on Robotics*, 31(2):400–414, April 2015. Conference Name: IEEE Transactions on Robotics.

[16] Matěj Karásek, Florian T. Muijres, Christophe De Wagter, Bart D. W. Remes, and Guido C. H. E. de Croon. A tailless aerial robotic flapper reveals that flies use torque coupling in rapid banked turns. *Science*, 361(6407):1089–1094, September 2018. Publisher: American Association for the Advancement of Science.

[17] J. James, V. Iyer, Y. Chukewad, S. Gollakota, and S. B. Fuller. Liftoff of a 190 mg Laser-Powered Aerial Vehicle: The Lightest Wireless Robot to Fly. In *2018 IEEE International Conference on Robotics and Automation (ICRA)*, pages 1–8, May 2018.

[18] Brunno Kuhn-Neto, Felipe A. L. Contrera, Marina S. Castro, and James C. Nieh. Long distance foraging and recruitment by a stingless bee, Melipona mandacaia. *Apidologie*, 40(4):472–480, July 2009.

[19] J.R. Riley, Don Reynolds, S. Mukhopadhyay, M.R. Ghosh, and T.K. Sarkar. Long-distance migration of aphids and other small insects in northeast India. *European Journal of Entomology*, 92:639–653, January 1995.

[20] Zhan Tu, Fan Fei, Limeng Liu, Yiming Zhou, and Xinyan Deng. Flying With Damaged Wings: The Effect on Flight Capacity and Bio-Inspired Coping Strategies of a Flapping Wing Robot. *IEEE Robotics and Automation Letters*, 6(2):2114–2121, April 2021. Conference Name: IEEE Robotics and Automation Letters.

[21] Andrew M. Mountcastle, Teressa M. Alexander, Callin M. Switzer, and Stacey A. Combes. Wing wear reduces bumblebee flight performance in a dynamic obstacle course. *Biology Letters*, 12(6):20160294, June 2016. Publisher: Royal Society.

[22] Crawford H. Greenewalt. The Wings of Insects and Birds as Mechanical Oscillators. *Proceedings of the American Philosophical Society*, 104(6):605–611, 1960.

[23] J. W. S. Pringle. The mechanism of the myogenic rhythm of certain insect striated muscles. *The Journal of Physiology*, 124(2):269–291, 1954.

[24] R. K. Josephson, J. G. Malamud, and D. R. Stokes. Asynchronous muscle: a primer. *Journal of Experimental Biology*, 203(18):2713–2722, September 2000.

[25] J. E. Molloy, V. Kyrtatas, J. C. Sparrow, and D. C. S. White. Kinetics of flight muscles from insects with different wingbeat frequencies. *Nature*, 328(6129):449–451, July 1987.

[26] K.E. Machin and J.W.S Pringle. The physiology of insect fibrillar muscle - II Mechanical properties of a beetle flight muscle. *Proceedings of the Royal Society of London. Series B. Biological Sciences*, 151(943):204–225, December 1959.

[27] ROBERT K. JOSEPHSON and DAVID YOUNG. A Synchronous Insect Muscle with an Operating Frequency Greater than 500 Hz. *Journal of Experimental Biology*, 118(1):185–208, September 1985.

[28] Douglas M. Swank, Vivek K. Vishnudas, and David W. Maughan. An exceptionally fast actomyosin reaction powers insect flight muscle. *Proceedings of the National Academy of Sciences*, 103(46):17543–17547, November 2006. Publisher: National Academy of Sciences Section: Biological Sciences.

[29] Bernadette M. Glasheen, Seemanti Ramanath, Monica Patel, Debra Sheppard, Joy T. Puthawala, Lauren A. Riley, and Douglas M. Swank. Five Alternative Myosin Converter Domains Influence Muscle Power, Stretch Activation, and Kinetics. *Biophysical Journal*, 114(5):1142–1152, March 2018.

[30] Jeff Gau, Nick Gravish, and Simon Sponberg. Indirect actuation reduces flight power requirements in Manduca sexta via elastic energy exchange. *Journal of The Royal Society Interface*, 16(161):20190543, December 2019. Publisher: Royal Society.

[31] S. P. Sane. The aerodynamics of insect flight. *Journal of Experimental Biology*, 206(23):4191–4208, December 2003.

[32] James Lynch, Jeff Gau, Simon Sponberg, and Nick Gravish. Dimensional analysis of spring-wing systems reveals performance metrics for resonant flapping-wing flight. *Journal of the Royal Society Interface*, February 2021. Publisher: The Royal Society.

[33] Douglas M. Swank. Mechanical analysis of Drosophila indirect flight and jump muscles. *Methods*, 56(1):69–77, January 2012.

[34] Torkel Weis-Fogh. Quick Estimates of Flight Fitness in Hovering Animals, Including Novel Mechanisms for Lift Production. *Journal of Experimental Biology*, 59(1):169–230, August 1973.

[35] M. B. BENNETT, R. F. KER, and R. MCN ALEXANDER. Elastic properties of structures in the tails of cetaceans (Phocaena and Lagenorhynchus) and their effect on the energy cost of swimming. *Journal of Zoology*, 1987.

[36] Jonas Buchli, Fumiya Iida, and Auke Ijspeert. Finding Resonance: Adaptive Frequency Oscillators for Dynamic Legged Locomotion. In *2006 IEEE/RSJ International Conference on Intelligent Robots and Systems*, pages 3903–3909, Beijing, China, October 2006. IEEE.

[37] Noah T. Jafferis, Moritz A. Graule, and Robert J. Wood. Non-linear resonance modeling and system design improvements for underactuated flapping-wing vehicles. In *2016 IEEE International Conference on Robotics and Automation (ICRA)*, pages 3234–3241, May 2016.